Available online at www.sciencedirect.com

ScienceDirect

International Journal of Plasticity 24 (2008) 2084–2101

INTERNATIONAL JOURNAL OF
Plasticity

www.elsevier.com/locate/ijplas

Experimental observations of evolving yield loci in biaxially strained AA5754-O

M.A. Iadicola *, T. Foecke, S.W. Banovic

National Institute of Standards and Technology, Gaithersburg, MD 20899-8553, USA

Received 12 July 2007; received in final revised form 29 February 2008
Available online 12 March 2008

Abstract

Experimental measurement of the plastic biaxial mechanical response for an aluminum alloy (AA5754-O) sheet metal is presented. Traditional methods of multiaxial sheet metal testing require the use of finite element analysis (FEA) or other assumptions of material response to determine the multiaxial true stress versus true strain behavior of the as-received sheet material. The method used here strives to produce less ambiguous measurements of data for a larger strain range than previously possible, through a combination of the Marciniak flat bottom ram test and an X-ray diffraction technique for stress measurement. The study is performed in conjunction with a study of the microstructural changes that occur during deformation, and these microstructural results are briefly mentioned in this work. Issues of calibration and applicability are discussed, and results are presented for uniaxial (U), plane strain (PS), and balanced biaxial (BB) extension. The results show repeatable behavior (within quantified uncertainties) for U to 20%, PS to almost 15%, and BB to above 20% in-plane strains. The results are first compared with three common yield locus models (von Mises', Hill'48, and Hosford'79), and show some unexpected results in the shape change of the yield locus at high strain levels (>5% strain). These changes include the rotation of the locus toward the von Mises surface and elongation in the balanced biaxial direction. Comparison with a more complex yield locus model (Yld2000-2d with eight adjustable parameters) showed that the locus elongation in the biaxial direction could be fit well (for a specific level of work), but at the detriment of fit to the plane strain data. Artificially large plastic strain ratios would be needed to match both the biaxial and plane strain behavior even with this more complex model.
Published by Elsevier Ltd.

---

* Corresponding author. Tel.: +1 301 975 5703.
E-mail address: mark.iadicola@nist.gov (M.A. Iadicola).

0749-6419/$ - see front matter Published by Elsevier Ltd.
doi:10.1016/j.ijplas.2008.03.003

Keywords: C. Mechanical testing; B. Anisotropic materials; A. Microstructures; B. Polycrystalline material; B. Metallic material

1. Introduction

Aluminum alloys have been receiving greater attention from the metal forming community in the last decade. AA5754 is of particular interest to the automotive industry for its high ductility, light weight, and strength. Unfortunately, the use of this material presents certain difficulties including surface roughening during deformation, occasionally yield point phenomena (including an initial yield plateau), and the Portevin–Le Chatelier (PLC) effect (Kang et al., 2006), which results in a serrated mechanical response during plastic yielding. However, these difficulties are surmountable, and the use of any alloy often is limited by its ability to be numerically modeled for an intended use. Many constitutive models exist based on extrapolation/prediction of multiaxial behavior from basic uniaxial tension tests, but these predictions often are insufficient to predict the actual biaxial material behavior (Ofenheimer et al., 2007).

Some constitutive models are calibrated using data from multiaxial tension and/or shear testing to achieve more accurate simulations (e.g., Vegter and van den Boogaard, 2006). However, the experimental data available are generally limited in both the strain states measured and the level of strains achieved. For example, Vegter and van den Boogaard (2006) combine the data from multiple methods of testing, yet still have to make certain assumptions in regards to the expected mechanical behavior to develop a broad enough data set for use in their model. Experiments using cylinders of material deformed by combined tension, torsion, and internal pressure are useful to develop data for a wide range of multiaxial strain states (Kuwabara et al., 2005), but would require the bending and welding of the material, thus changing the material's initial condition and behavior. Biaxial tension data for sheet metal samples can be generated using cruciform specimens (e.g., Kuwabara et al., 2002; Banabic, 2004), bulge testing (e.g., Gutscher et al., 2004), or wide strip testing (which is capable of achieving strain states from plane strain to simple shear, e.g., Flores et al., 2007), but each technique has aspects that limit its accuracy, whether it is the assumption of a constitutive law when using finite element analyses to interpret the results or uncertainties due to out of plane bending and inhomogeneous strain fields.

The purpose of this study is to produce less ambiguous stress–strain measurements during large strain in-plane (biaxial) stretching of an as-received aluminum alloy (AA5754-O) sheet metal sample. These results can then be compared with common model predictions of yield loci (in stress space) at various plastic strain levels. A variation of the Marciniak flat bottom ram test is used to impose near-linear strain paths. This method permits application of strain paths from uniaxial through plane strain to balanced biaxial (for plane stress samples). Often this range of deformations requires multiple testing methods (Kuwabara, 2007; Vegter and van den Boogaard, 2006), each with its own dissimilar assumptions, thus leading to a potentially inconsistent data set. The method used here produces data that is measured in a self-consistent way. This method incorporates unquantifiable friction forces, thus there is no simple relation between the stress in the sheet and the ram force. This problem is overcome by the use of X-ray diffraction (XRD) in a manner similar to residual stress measurement to determine the *in situ* stress in the sheet.

2. Experimental technique

Below is a brief description of the material to be studied, and descriptions of the two types of experiments to be performed: (1) standard tensile uniaxial fixed-rate tests and (2) tensile multiaxial experiments with pauses in loading during which X-ray diffraction measurements are made. The standard uniaxial tests are for comparison with the XRD results, and are the typical/basic tests used to calibrate models for biaxial simulation in the absence of multiaxial experimental data.

2.1. Material

The material used in this investigation is commercially available AA5754-O sheet. The chemical composition determined using ASTM standard E227 is reported in Table 1. The microstructure of the as-received sheet in the O-temper shows recrystallized grains, Fig. 1. The size of the grains is relatively uniform in all three directions with those in the normal plane having an average diameter of 39 μm ± 6 μm, measured by the linear intercept method (ASTM E112, with one standard deviation of uncertainty). Their shape is relatively equiaxed in the rolling plane, but slightly elongated when viewed in the transverse plane. The macrotexture of the as-received material is measured using an X-ray diffraction technique on a conventional diffractometer with quarter Euler cradle. Cu $K\alpha$ radiation (wavelength $\lambda = 0.1541$ nm) is used to illuminate the samples with a multiwire area detector collecting the signal. The three-dimensional orientation distribution function (ODF), Fig. 2, is expressed by Euler angles, ϕ_1, Φ, and ϕ_2 (in Bunge's notation), which relate

Table 1
Chemical composition of AA5754, as mass fraction multiplied by 100

Si	Fe	Mg	Mn	Cu	Zn	Cr	Al
0.06	0.24	3.56	0.28	0.05	0.05	0.05	Balance

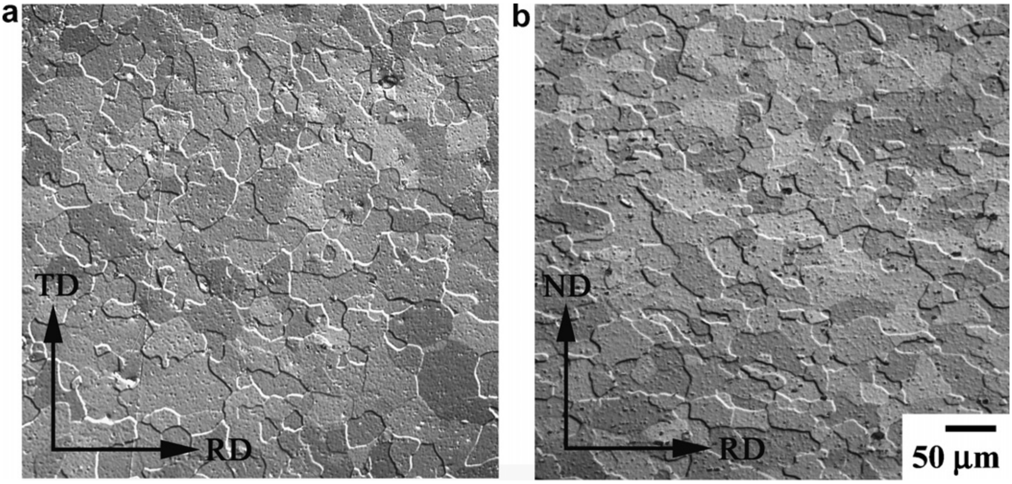

Fig. 1. Optical micrographs (a) normal and (b) transverse to the rolling plane for the as-received material.

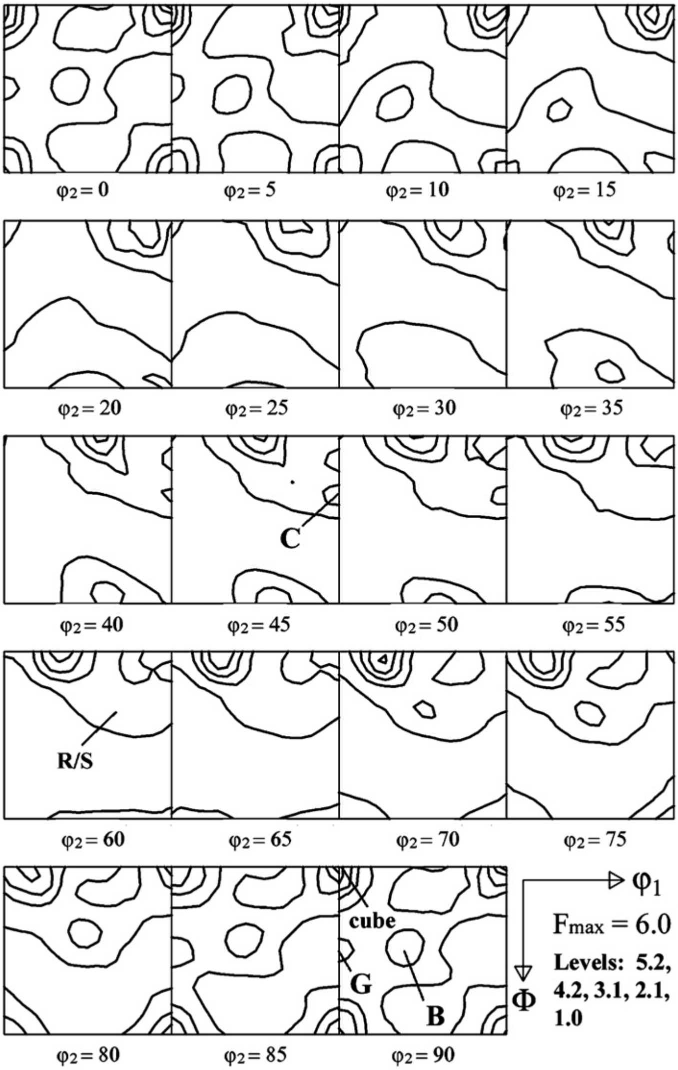

Fig. 2. Orientation distribution function of as-received AA5754-O, with ϕ_1 and Φ axes running from 0° to 90°. Positions of ideal orientation are shown (Cube, R, Goss, Brass, S, and Copper).

the cubic crystal frame to the orthotropic sample frame given by the normal direction (ND), the rolling direction (RD), and the transverse direction (TD), respectively. Recrystallization components (Cube and R orientations), as well as a significant fraction of rolling texture components (Brass and Copper orientations), are observed.

2.2. Uniaxial experiments

Uniaxial (U) tests using ASTM E8 sub-size specimens (Fig. 3) are performed using a 88 kN electro-mechanical testing frame. Load during the testing is monitored using a calibrated 4.5 kN load cell. Strains are measured using two calibrated extensometers (one

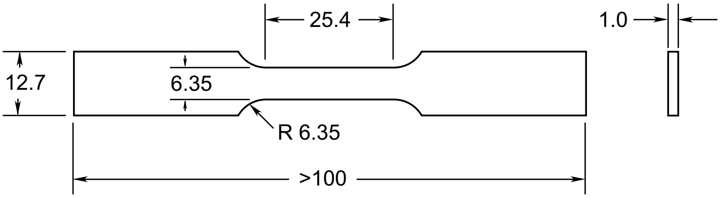

Fig. 3. Uniaxial specimen with dimensions shown in mm.

axial with a 10 mm gage length, and one transverse, across the width). Due to the PLC banding seen in the material response and the resulting local inhomogeneous plastic strain, control of the test is based on grip displacement, resulting in an average strain rate of $6 \times 10^{-4}\ \mathrm{s}^{-1}$.

2.3. Biaxial experiments

The multiaxial tension experiments are performed using a variation (Raghavan, 1995) of the Marciniak (Marciniak and Kuczyński, 1967) flat bottom ram test where each sheet metal specimen is reinforced outside of the gage section with a sacrificial washer sheet (in this case made of a mild steel). A modified 500 kN capacity servohydraulic mechanical testing frame (Foecke et al., 2001) is used with specialized tooling (cylindrical ram and binder, Fig. 4) to perform the experiments. Balanced biaxial (BB) states of strain are achieved with a 305 mm square specimen and washer (with a 32 mm diameter hole). Near-linear strain paths for other strain states are realized using a similar geometry, but with a reduced specimen width along the direction of reduced straining (Raghavan, 1995). For example, near plane strain (PS) conditions are achieved here using a specimen width of 135 mm (with a longitudinal length of 305 mm), resulting in strain in the longitudinal direction while having near zero strain in the transverse direction (width). Due to the hole in the washer and a recess in the center of the ram (Fig. 4), the gage section (center) of the specimen is stress free on the upper and lower surfaces. Strain is measured using a calibrated biaxial extensometer (Class C, ASTM E83-92, accuracy throughout the 40% strain extensometer range).

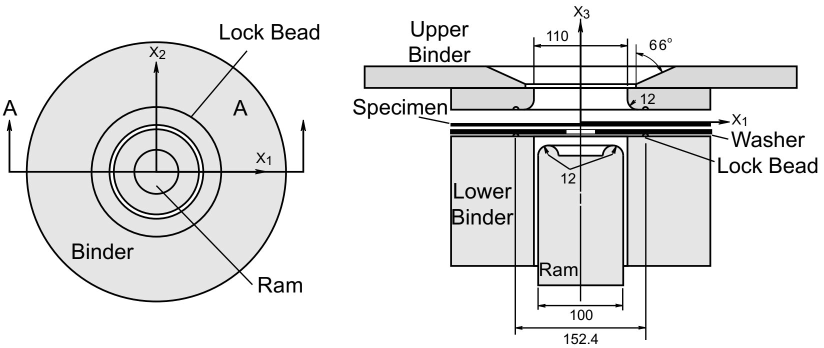

Top View

A-A

Fig. 4. Marciniack tooling (dimensions shown in mm) with specimen inserted in cross-section view (right).

As mentioned earlier, due to the presence of unquantifiable friction forces, no simple relation between ram force and applied stresses exists. Therefore, a method of stress determination (often referred to as the "$\sin^2\psi$ method") using XRD methods and equipment originally developed for residual stress measurement is used. This method (described in Foecke et al., 2007), uses an X-ray beam source (typically Co $K\alpha$ or Cr $K\alpha$) diffracted from a sampled volume on the surface of the specimen to measure the interatomic spacing (through Bragg's Law) from a set of atomic planes at a specific orientation. This method samples only the crystallites in the diffracted volume with a specific selected crystallographic orientation with respect to the beam and detector (Fig. 5). By tilting the beam and detector an angle (ψ) to the surface normal, a different set of crystallites within the diffracting volume will be sampled. By oscillating the ψ angle slightly ($\pm 3^\circ$), the number of crystallites sampled are increased within the neighborhood of the ideal orientation of interest. This results in a peak profile observed using two-256 channel, 10° position sensitive scintillation detectors (one placed symmetrically on each side of the source beam). The individual detector channels are calibrated using a scan of an amorphous target (a glass slide in this case). After detector gain correction, a background level is determined based on two points selected outside of the peak limits. In the current work, the upper 85% of the peak is fit to a Pearson's VII function (with an exponent of 1.77), after the background level of the profile is subtracted. Peak broadening (due to an increase in dislocation density during plastic deformation) may not allow for proper background determination. Care is taken to ensure that for each measurement the peak width is never more than half of the detector width, and that the tails of the peak are not cropped by the limits of the detector. For all the *in situ* XRD data shown here, the source radiation is the Co $K\alpha$ (wavelength $\lambda = 0.1790$ nm), and the reflection is for the {420} family of planes (Bragg angle $2\theta = 162.5^\circ$).

The individual crystallites sampled respond elastically to the applied load even during dislocation motion, and after the specimen is yielded through the thickness, the surface

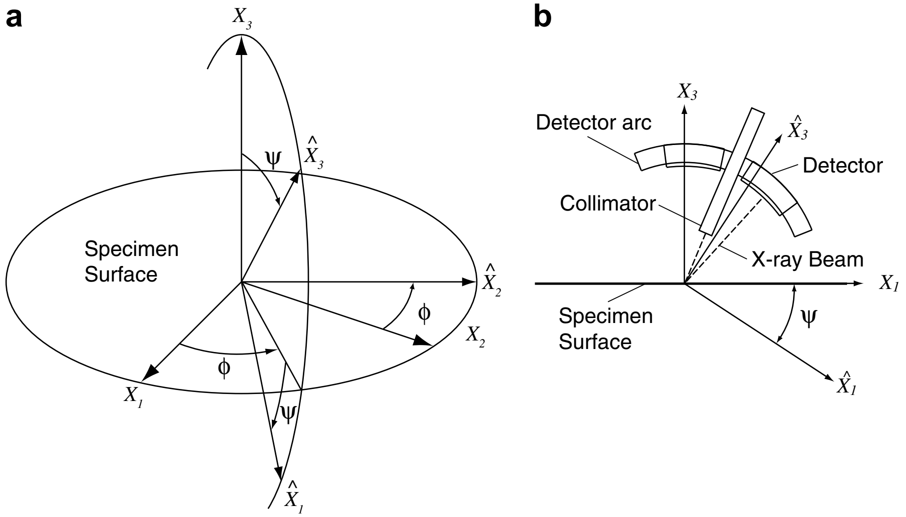

Fig. 5. XRD axes definition, where (a) is the general definition and (b) is for $\phi = 0^\circ$ and shows the X-ray beam, collimator, and detector locations. The X axes define the specimen system, and the $\widehat{X}$ axes define the detector system.

stress equals the macroscopic flow stress through the thickness. The diffracting volume must be chosen sufficiently large to incorporate a representative sample of crystallites in various crystallographic orientations. Here the focal spot illuminated is 5 mm long and 1.5 mm wide (in the ψ tilt direction) with a maximum penetration depth of approximately 40μm. This results in a diffracting volume encompassing approximately 4500 grains (based on the average grain size). The intensity variation with position on the surface of an as-received sample may be used to approximate the number of crystallites sampled (Gnaeupel-Herold et al., 2004) for a given ψ tilt angle. A limited data set of these intensities for our material results in a conservative sampling estimate of greater than 150 grains for almost all of ψ tilt angles used, and never less than 70 grains. Although the data set is too limited to achieve statistically significance, even the conservative estimate is sufficiently large to be a representative sampling, and this adequacy is reinforced by the quality of the diffraction peaks measured throughout this study.

The standard governing equation relating the lattice strain to the surface strains (Noyan and Cohen, 1987) in the surface system (Fig. 5a) where the X_1 axis parallel to the rolling direction of the sheet is

$$\frac{d_{\phi\psi}-d_o}{d_o} = \varepsilon_{11}\cos^2\phi\sin^2\psi + \varepsilon_{12}\cos 2\phi\sin^2\psi + \varepsilon_{22}\sin^2\phi\sin^2\psi + \varepsilon_{33}\cos^2\psi + \varepsilon_{13}\cos\phi\sin 2\psi + \varepsilon_{23}\sin\phi\sin 2\psi, \quad (1)$$

where d is the interatomic lattice spacing determined through Bragg's Law, ϕ (the rotation about X_3) and ψ (the rotation about $\widehat{X}_2$) are the orientation angles, and ε_{ij} are the components of strain in the surface system. The stress-free lattice spacing (d_o) is not measured directly, since the "$\sin^2\psi$ method" is not very sensitive to error in this value, and a system default value for d_o of aluminum is assumed. To verify this, an XRD measurement of a stress-free aluminum powder is made, and the assumed d_o is considered acceptable if the measured stress is less than the uncertainty of the measurement.

Since the top and bottom surfaces of the specimen are stress free in the center region of interest, we neglect the through thickness stress $(\sigma_{33}=0)$. Assuming an isotropic constitutive law and tilting in the rolling direction $(\phi = 0^\circ)$ Eq. (1) becomes

$$\frac{d_\psi - d_o}{d_o} = S_2\sigma_{11}\sin^2\psi + S_1(\sigma_{11}+\sigma_{22}) + S_2\sigma_{13}\sin 2\psi \quad (2)$$

and if the tilt is in the transverse direction $(\phi = 90^\circ)$

$$\frac{d_\psi - d_o}{d_o} = S_2\sigma_{22}\sin^2\psi + S_1(\sigma_{22}+\sigma_{11}) + S_2\sigma_{23}\sin 2\psi, \quad (3)$$

where $S_1 = -\frac{v}{E}$ and $S_2 = \frac{1+v}{E}$. S_1 and S_2 are the effective X-ray elastic constants (XECs) whose values are associated with a chosen family of planes $(\{hkl\})$ in a specific material, and may be affected by alloying or crystallographic texture (Noyan and Cohen, 1987), as well as by other less significant variables. It is reasonable to assume that the effective XECs will differ for the rolling and transverse directions; therefore we experimentally calibrate for S_2 in each of these directions. We are most concerned with the stress in the direction of tilt (ψ) and will perform multiple tests to obtain the stress in each of the first two principal strain directions, which are chosen here to coincide with the rolling or transverse directions of the sheet material. These measurements will require calculation of the slope of the lattice strain – $\sin^2\psi$ relationship, but not the intercept, thus S_1 does not need to be determined. (Note: although the second terms in Eqs. (2) and (3) are not measured, they are used by the XRD system to permit the combination of the data from the two detectors by assuming a common intercept in the lattice strain – $\sin^2\psi$ behavior.) Since the top and bottom surfaces of the sample are stress free and the measurements are made after the initial yielding of the material, no shear stresses σ_{13} or σ_{23} should exist, and any lattice strain variation with $\sin 2\psi$ is a result of systematic errors or micro-stresses. In our results, these effects are minor (within the uncertainty of the XRD measurements), and therefore are not discussed further.

The central procedure for the Marciniak-style testing performed here includes three steps: (1) the material is loaded by an increase in ram height at a quasistatic rate, (2) the ram position is held and the XRD system is focused on the surface of the sheet, and (3) a scan of selected ψ angles (13 in this case) is taken each with a small (±3°) oscillation and an associated peak location (θ angle) may be calculated (as well as the lattice spacing through Bragg's Law). At this point the stress may be calculated from the XRD data. The macroscopic strain during this hold time is calculated by averaging the output of the biaxial extensometer for the entire scan time, and typically has a standard deviation <0.005% strain (which is 10 times larger than the typical fixed error associated with the extensometer). This procedure can then be repeated for the next data point. The entire procedure (1 through 3) takes approximately 8 min with each peak profile taking about 15 s. This is due to the low power of the X-ray tube (60 W) and X-ray absorption by the aluminum. Note: the XRD method of stress measurement described above is generally applicable, and although it is used here in conjunction with the Marciniak method of imposing strains on an aluminum alloy, it could also be applied to other materials and methods of biaxial straining (e.g., cruciform testing) as long as the material has been yielded through the thickness without substantial gradients in stress through the thickness.

Effective XEC calibration experiments are performed using the uniaxial ASTM E8 subsize specimens (Fig. 3) prepared in the same manner as the specimens mentioned above. A portable mechanical testing frame is used to strain the samples while under the XRD system. Load (measured using a calibrated load cell) and strain (measured using an axial extensometer) are used to determine the true stress in the gage section. At selected strain levels the specimen is unloaded (to a level never less than 80% of the initial uniaxial yield) and reloaded elastically. During these elastic unload/reload times, the uniaxial loading is paused at multiple points and XRD is used to measure the current stress. By comparing the XRD and load cell measured values, the calibrated effective XECs may be determined. For this work, the average effective XECs are determined by averaging all of the XECs measured for each elastic unload/reload (7–8) during one uniaxial test in each direction (RD and TD). Since texture evolves during plastic deformation (Banovic and Foecke, 2003; Banovic et al., 2008) and effective XECs may be texture dependent, it would be expected that these values vary with strain or stress level and/or path. This has been shown to be a minor effect in this case (Iadicola and Gnaeupel-Herold, 2008) and a detailed discussion is beyond the scope of this work.

3. Results

Stress–strain curves for the standard tensile uniaxial fixed rate tests are shown in Fig. 6 for the rolling (RD), transverse (TD), and 45° diagonal (DD) directions. Three tests are performed for each direction, and all result in nearly identical curves. Therefore, only

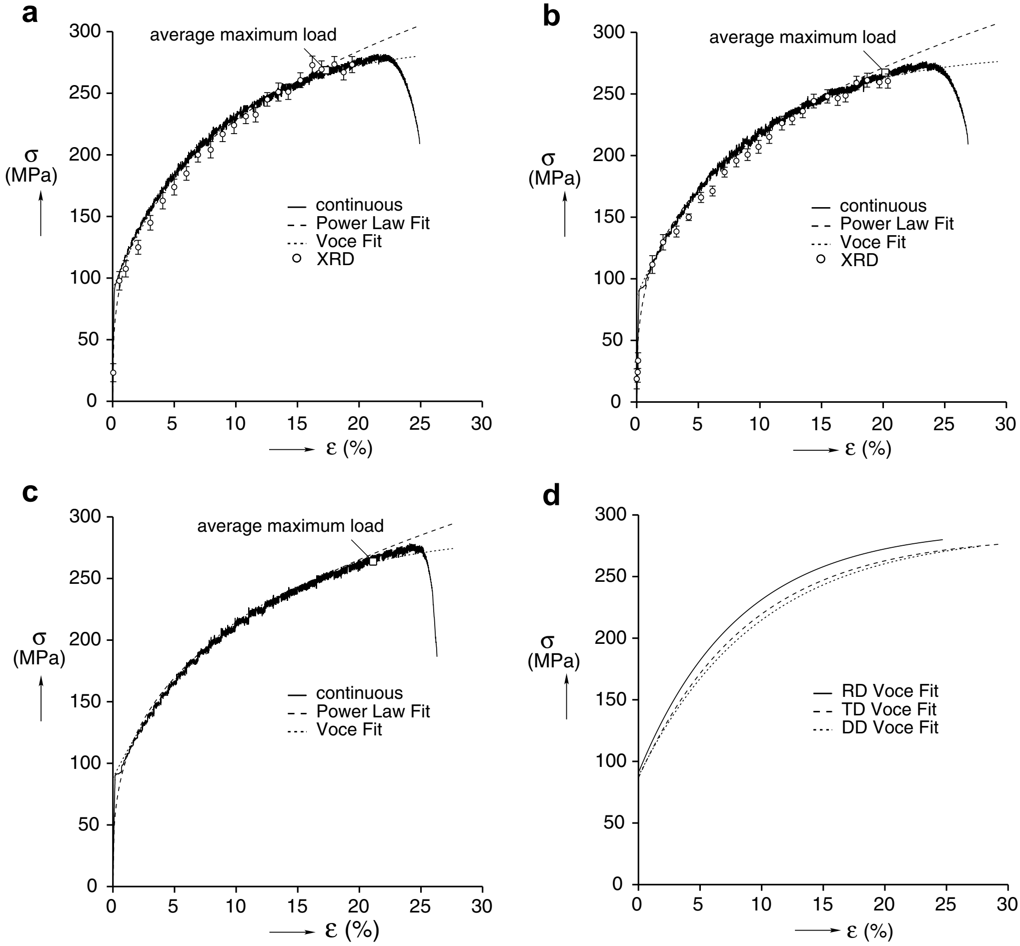

Fig. 6. Uniaxial true stress–true strain curves for specimen (a) 0°, (b) 90°, and (c) 45° to the rolling direction, and (d) the Voce fits for all three orientations plotted together. Data points (circles) are the result of uniaxial experiments incorporating the XRD system.

one representative curve is shown in Fig. 6 for each orientation. These data are fit with power law ($\sigma = K\varepsilon^n$) and Voce ($\sigma = S_\infty(1 - Ae^{B\varepsilon})$) hardening models over the applicable plastic range (above the initial yield and below the maximum uniform elongation), and are shown as dashed and dotted lines, respectively in Fig. 6 (Table 2 lists the average values of these model variables, calculated from the three repeat tests). The Voce fits for all three directions are plotted together in Fig. 6d to better show the relative position of the data plotted in Fig. 6a–c. Since PLC banding occurs, the elongation is only truly uniform in the elastic region, but we assume a definition of the maximum uniform elongation based on the maximum point of the engineering load displacement curve. A further adjustment is made in selecting the maximum point of the engineering load displacement curve. Since the serrated yielding (seen throughout the plastic yield regime) tends to cause sudden local maxima and local minima, the actual maximum load recorded may be the effect of local

Table 2
Basic uniaxial material properties

		Units	RD	TD	DD
0.2% Yield stress		MPa	94.1 [3.3]	92.1 [0.7]	90.9 [0.6]
Tensile strength		MPa	226 [3]	218 [1]	216 [3]
Maximum uniform elongation		%	18.9 [0.9]	21.5 [0.5]	22.4 [0.9]
q			0.409 [0.005]	0.464 [0.005]	0.422 [0.010]
r			0.69 [0.02]	0.87 [0.02]	0.73 [0.03]
Power law fit[a]	K	MPa	474 [9]	458 [6]	447 [3]
	n		0.317 [0.010]	0.326 [0.006]	0.323 [0.004]
Voce fit[b]	S_∞	MPa	289 [2]	284 [2]	286 [3]
	A		0.686 [0.014]	0.695 [0.007]	0.693 [0.004]
	B		−12.3 [0.3]	−11.2 [0.2]	−10.2 [0.5]

Uncertainties (shown in brackets) are based on one standard deviation.

[a] $\sigma = K\varepsilon^n$.

[b] $\sigma = S_\infty(1 - Ae^{B\varepsilon})$.

PLC banding and not the overall response of the material. Therefore, the maximum uniform elongation and stress at that point are determined using the median values of true stress and true strain within the range of data points where load is within 22 N (approximately equal to twice a typical load drop due PLC motion) of the actual maximum load. This method greatly reduces the scatter between the three repeat tests in the variables shown in Table 2.

The contraction ratio (a plastic analog to the Poisson's ratio in elasticity, defined as the negative of the width strain, ε_w, over the longitudinal strain, ε_l) is reported in Table 2 where the value is averaged for the three experiments performed in each orientation over the applicable plastic range (described above). The average value of r (the plastic strain ratio, equal to the width strain, ε_w, over the thickness strain, ε_t) as defined in ASTM E517-92 is similarly calculated, where ε_t is calculated from the measured strains assuming constant volume during plastic deformation. The uncertainties reported for these ratios are the standard deviations between the three experimental results for each orientation, and not the variation seen in one experiment. The averaging for each experiment individually is required, since the transverse extensometer monitors the width of the specimen over a much smaller amount of the axial length than the axial extensometer, resulting in oscillations throughout the plastic range of the q and r values (as shown in Fig. 7) resulting from the PLC banding.

Additional uniaxial experiments are performed using a portable mechanical testing frame with the XRD system. These are used to compare with the standard uniaxial curves and to check the calibrated effective XECs ($S_2^{\mathrm{RD}} = 19.3 \pm 0.9\ \mathrm{TPa}^{-1}$, $S_2^{\mathrm{TD}} = 19.7 \pm 0.7\ \mathrm{TPa}^{-1}$). The data are plotted as points along with the standard uniaxial experiments in Fig. 6a and b. The data match well with only a slight deviation between 5% and 12% strain for both the RD and TD. This may be in part due to the effect of texture changes during plastic deformation, and is discussed in Iadicola and Gnaeupel-Herold (2008). Although the texture change itself was shown to have a minor effect, the subsequent intergranular stresses that arose were measurable, but close to the resolution of the XRD system. The resulting variation in the XECs was deemed minor in comparison to the uncertainty of the measurement (Iadicola and Gnaeupel-Herold, 2008) and therefore is neglected here. The error bars shown in Fig. 6a and b are based upon the quality

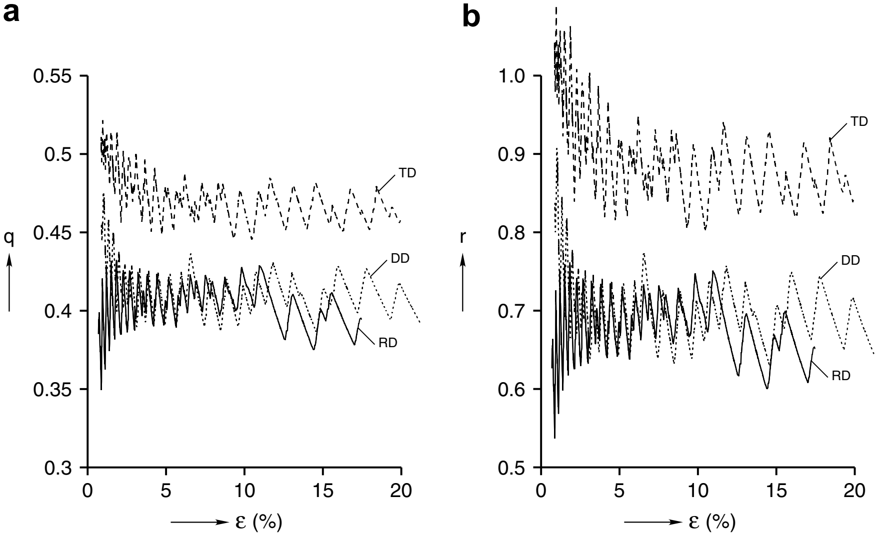

Fig. 7. Plastic strain ratios (a) q and (b) r variation with true strain (in applicable plastic region) for specimen 0° (RD, solid line), 90° (TD, dashed line), and (c) 45° (DD, dotted line) to the rolling direction. Results are for the same experiments as shown in Fig. 6.

of the linear fit of the lattice strains versus $\sin^2\psi$. The size of the error bars are not much larger than the stress variations resulting from the serrated yielding. The XRD data values are predominantly at the lower edge of the serrated hardening curve, which seems intuitive considering they are measured during pauses in loading. The load rises and drops are associated with PLC band creation and motion (both transient events). The same uniaxial data are plotted in Fig. 8a along with the data for the PS and BB tests shown in gray for comparison. The points are connected by lines to aid visibility, but these lines are not intended to suggest the actual stress strain path between the points.

The results for the plane strain (PS) experiments using XRD are plotted in Fig. 8b, for both maximum strain in the rolling direction (PS in RD) and the transverse direction (PS in TD). The PS stress data for the near zero strain direction (with measured strain ratios typically <0.05) are plotted using the strain in the maximum (principal) strain direction for visibility, and are the sets of points below 100 MPa. The XECs used are the same as those for the uniaxial experiments above. Since the XRD method only measures the stress in one direction for each experiment performed, two experiments are needed to obtain (1) the stress in the direction of principal strain and (2) the stress in the other (near zero strain) direction within the plane of the sheet. Two experiments (one original and one repeat) are performed for each direction (the maximum strain direction and the near zero strain direction) for a total of eight experiments shown in Fig. 8b. Repeat experiments are performed by a different system operator four months after the first set in order to verify the repeatability of the experimental method. There is a slight difference between the results of the repeat experiments, but most are within the error bars of the data. The trends are quite consistent; for example the stress in the near zero strain direction is always higher in the "PS in TD" experiments than in the "PS in RD" experiments.

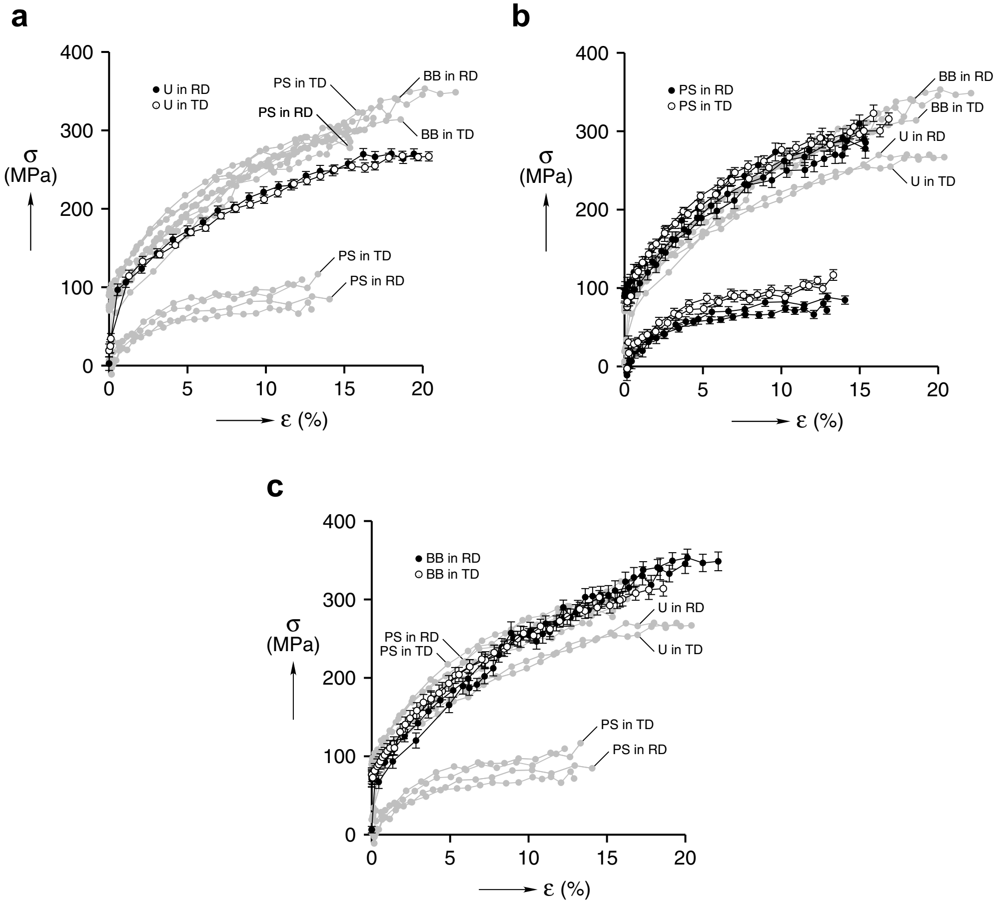

Fig. 8. Multiaxial true stress–true strain curves determined through XRD for (a) U, (b) PS, and (c) BB experiments with other experiments shown in gray for comparison. PS stress data for the near zero strain direction are plotted using the first principal strain for visibility.

The balanced biaxial experimental results are plotted in Fig. 8c for the sheet texture directions (RD and TD). Again a separate experiment is performed for each direction and repeat experiments are performed similarly to those above, all using the same uniaxially determined XECs. The repeat experiments show good agreement with the exception of one data point in the RD at about 2.7% strain, which appears to be about 15 MPa too low. The general trend is that the stress in the TD is initially higher than the RD up to 5% strain at which point the trend reverses and the RD stress is higher.

As mentioned earlier, the "$\sin^2 \psi$ method" for stress determination can be sensitive to the presence of crystallographic texture, as texture will have a tendency to increase (or decrease) the number of grains oriented at the Bragg condition for a given tilt, thereby increasing (or decreasing) the diffracted X-ray signal. Additionally in some materials, texture has been shown to cause the unusual nonlinearity in the lattice strain – $\sin^2 \psi$ relationship (e.g., for iron or steel Dölle et al., 1977; Marion and Cohen, 1974). Additional samples of AA5754-O are

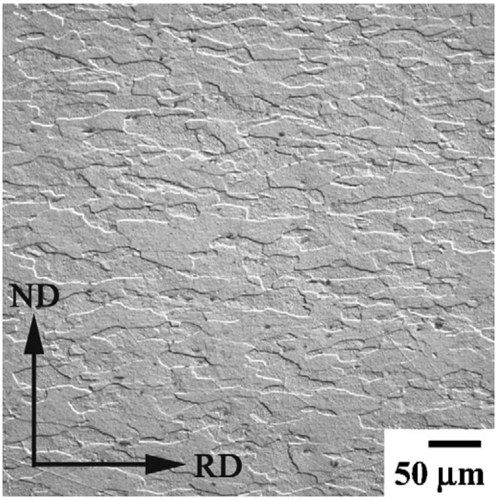

Fig. 9. Optical micrograph of 20% balanced biaxial strained sample transverse to the rolling plane.

prestrained (using the same Marciniak tooling) to intermediate strain levels (5%, 10%, 15%, and 20%) for microscopy and macrotexture analysis. Fig. 9 shows a cross-section of the AA5754-O sheet strained to 20% in-plane plastic strain. The elongation of the grains, due to plastic deformation, is obvious if compared to Fig. 1b. Fig. 10 shows three ϕ_2-sections for the as-received material and those resulting after biaxial extension (to 5%, 10%, 15%, and 20% strain). For a complete review of the changes seen in texture and microscopy for the material in this study, see Banovic et al. (2008). In Fig. 10 some orientations are noticeably strengthened (components in the $\langle 011\rangle_{ND}$-fiber, $0^\circ \leqslant \phi_1 \leqslant 90^\circ$, $\Phi = 45^\circ$, and $\phi_2 = 90^\circ$) and others weakened (recrystallization components, R, Cube). Despite these distinct changes in texture (e.g., the decrease in Cube texture is greater than four times the random distribution) and grain shape, the method does not show any catastrophic loss of signal or non-linear $\sin^2\psi$ behavior for this alloy.

4. Discussion

Fig. 11 is a plot of the multiaxial data interpolated into levels of constant plastic work on stress axes. The data points are developed using the data in Fig. 8 and the definition of plastic work as

$$W = \int \left(\sigma_{ij} - \frac{1}{3}\sigma_{kk}\delta_{ij}\right) d\left(\varepsilon^p_{ij} - \frac{1}{3}\varepsilon^p_{kk}\delta_{ij}\right), \tag{4}$$

where the first term on the right hand side is the deviatoric stress, the second term in the deviatoric plastic strain, and the indices range from 1 to 3 (with repeated indices indicating summation). Assuming constant volume during plastic straining, this may be simplified to

$$W = \int \left(\sigma_{ij} - \frac{1}{3}\sigma_{kk}\delta_{ij}\right) d\varepsilon^p_{ij}, \tag{5}$$

where plastic strain (ε^p) is calculated using the measured true strain and true stress $\left(\varepsilon^p_{ij} = \varepsilon_{ij} - \frac{1+\nu}{E}\sigma_{ij} + \frac{\nu}{E}\sigma_{kk}\delta_{ij}\right)$ assuming elastic constants $E = 70$ GPa and $\nu = 0.33$. Since

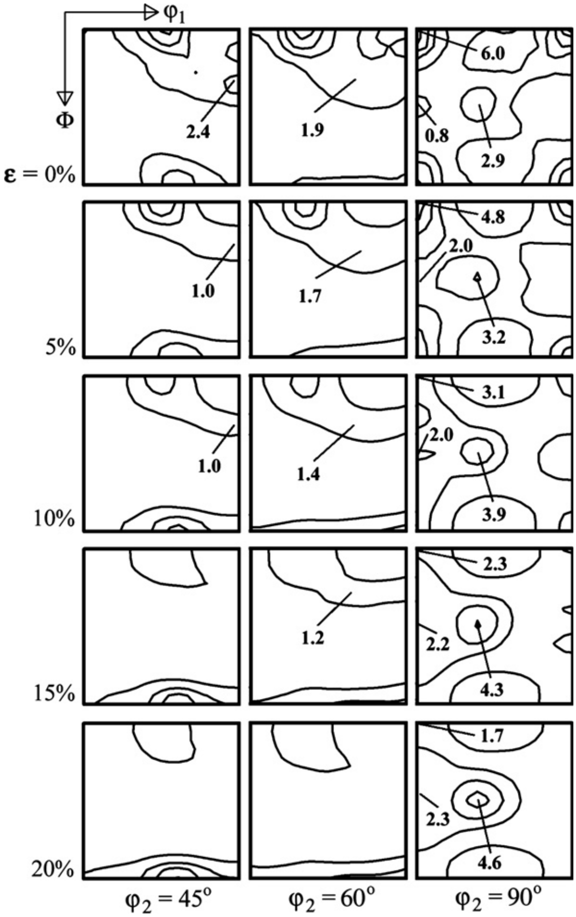

Fig. 10. Selected ODF ϕ_2-sections for as-received material and after biaxial straining to four strain levels (5%, 10%, 15%, and 20%), with ϕ_1 and Φ axes running from 0° to 90°.

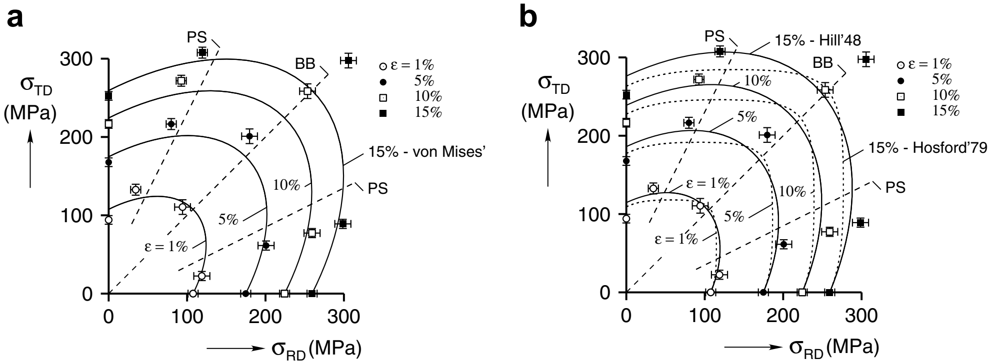

Fig. 11. Data from Fig. 8 interpolated onto stress axes (data points) for comparison to (a) von Mises' (solid lines), (b) Hill'48 (solid lines) and Hosford'79 (dotted lines) model yield surfaces based on the uniaxial experimental results. Dashed lines show the isotropic prediction for PS and BB strains.

the data in Fig. 8 is not continuous (and from as many as 4 different tests for one strain state), interpolated curves for each data set (with some minor smoothing) are used to calculate the resulting plastic work. The values of plastic work per unit volume calculated for the uniaxial RD at 1%, 5%, 10%, and 15% strain levels are used as the work contour values of interest (with values of $0.69\ \mathrm{MJ/m^3}, 6.43\ \mathrm{MJ/m^3}, 16.52\ \mathrm{MJ/m^3}$, and $28.60\ \mathrm{MJ/m^3}$, respectively). For these strain levels, the yield surfaces are calculated and plotted for three models: von Mises' (solid line in Fig. 11a), Hill'48 (Hosford and Caddell, 1983, pp. 266 ff., solid line in Fig. 11b), and Hosford'79 (Hosford and Caddell, 1983, pp. 269 ff., dotted line in Fig. 11b, where the model parameter $a = 8$ is used for an FCC material) using the plastic strain ratios, r values, from Table 2 when required by the models. The yield locus data points plotted are those calculated from the data shown in Fig. 8 for the same plastic work values of interest. The dashed lines in Fig. 11 show the location of the predicted PS and BB data based on isotropic material behavior.

The XRD data for PS in the TD and RD are consistently offset from the isotropic prediction toward the uniaxial stress axes, where the offset is greater in the case of PS in the RD. However, both sets of data lie on or close to the von Mises' and Hill'48 curves. For PS in the TD, Hill'48 (which incorporates the anisotropy using the r values in Table 2) is closer to the data then von Mises', but the Hill'48 does not match the data for PS in the RD or U in the TD as well as the von Mises' model. The BB XRD data matches the isotropic prediction well (generally following the $\sigma_{\mathrm{RD}} = \sigma_{\mathrm{TD}}$ dashed line) with some minor variation, but does not match any of the model curves in value, especially for the 10% and 15% points (biaxial strains where data has typically been previously unavaliable for sheet metal). There is some movement of the points from the $\sigma_{\mathrm{RD}} < \sigma_{\mathrm{TD}}$ to $\sigma_{\mathrm{RD}} = \sigma_{\mathrm{TD}}$ with increased plastic work. The data suggests that the shape of the yield locus does not remain constant with increasing plastic strain level, and thus does not match any of the models (whether isotropic or anisotropic). The initial yield locus is flattened slightly in the balanced biaxial direction, and more convex toward the transverse stress direction near the measured plane strain data. As plastic straining proceeds, the shape of the locus elongates in the balanced biaxial direction substantially, while the other points approach or remain close to the von Mises' curves and to a lesser extent the Hill'48 curves. None of the models match the BB stresses above the 1% strain level. Note: similar BB behavior is seen in steels, but steel r values are >1 unlike aluminum alloys (values in Table 2 are more typical). Artificially large r values could be used to adjust the model predictions closer to the yield locus data, but the r values would have no physical significance.

These yield locus changes are more clearly seen when plotting the differential hardening where the axes are normalized by the uniaxial RD stresses at the same plastic work levels

$$\bar{\sigma} = \frac{\sigma}{\sigma_{\mathrm{RD}(\sigma_{\mathrm{TD}}=0)}} \tag{6}$$

as shown in Fig. 12. Where as the model curves each collapse to a single curve, the yield points for each plastic work level (1%, 5%, 10%, and 15% strain) tend to shift closer to the von Mises' curve for both PS directions and for U in the TD, but the BB points rotate toward $\bar{\sigma}_{\mathrm{RD}} = \bar{\sigma}_{\mathrm{TD}}$ while extending further out from the model curves. This shows that for these strain states the material behaves less anisotropically at higher strain levels (moving from orthotropic behavior to an almost specially orthotropic response). In all cases, the major shift is seen between the 1% and 5% levels and almost no change is present between the points associated with the 10% and 15% levels. In Kuwabara et al. (2005),

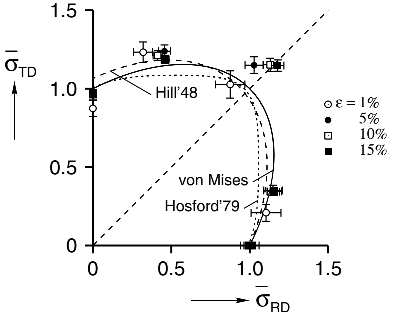

Fig. 12. Data from Fig. 11 normalized by uniaxial yield stresses in the rolling direction with the von Mises' (solid curve), Hill'48 (dashed curve), and Hosford'79 (dotted curve) predictions. The dashed line traces equal stress in RD and TD, for reference.

a different 5000-series aluminum alloy (initially processed into tubes) is deformed by combined pressurization and tension, and the data showed BB strain resulted in a σ_{RD} to σ_{TD} ratio of 20:23 (0.87) for all the plastic strain levels from 0.2% to 25%. The results in Figs. 11 and 12 have σ_{RD} to σ_{TD} ratios of 0.85, 0.89, 0.98, 1.03 for 1%, 5%, 10%, and 15% strain, respectively, and when including the intermediate strain levels (not plotted) the largest changes are seen between 6% and 8% strain after which the ratios fluctuate in a range of 0.98 to 1.03 (where $\bar{\sigma}_{RD} = \bar{\sigma}_{TD}$ is within the uncertainties of the data points). Additionally, the results described in Kuwabara et al. (2005) do not show $\bar{\sigma}_{RD} > 1$ and $\bar{\sigma}_{TD} > 1$ as seen here. It is not clear if these differences are a result of the different material tested (alloy and heat treatment) or the test configuration (sheet/tube) and its required assumptions.

A model that admits normalized BB stresses >1 is Yld2000-2d (Barlat et al., 2003). This model is typically calibrated (as described in Barlat et al., 2003) using standard uniaxial tests (in the RD, TD, and DD) and a balanced biaxial stress test (where the strain ratio of two directions is defined as $r_b = d\varepsilon_{TD}/d\varepsilon_{RD}$). An average r_b value of 1.13 is determined from the data in Fig. 8c. The stress values for the model calibration are taken from the data in Fig. 12 with the exception of the uniaxial DD values which are determined from the data in Fig. 6c with the stress values reduced by 6.5 MPa to center the data on the lower edge of the PLC load drops similar to the XRD data (shown in Fig. 6a and b and discussed in Section 3) such that the uniaxial DD curve is very close to or below the uniaxial XRD TD data shown in Fig. 8a similar to the relative curve (dotted and dashed) locations shown in Fig. 6d. The resulting model parameters (using $a = 8$ for FCC material, as before) calculated for the 15% data in Fig. 12 are

$$\alpha_1 = 0.8319, \quad \alpha_2 = 1.0765, \quad \alpha_3 = 0.6731, \quad \alpha_4 = 0.9592,$$
$$\alpha_5 = 0.9530, \quad \alpha_6 = 0.6520, \quad \alpha_7 = 0.9784, \quad \text{and} \quad \alpha_8 = 1.4059$$

and the associated yield locus curve is plotted in Fig. 13b (Case 1, solid line). Because the model calibration uses the BB and U data these data are matched well. The model predictions for PS, however, are far off of the experimental data. Using artificially high values of $r_{RD} = 1.5$ and $r_{TD} = 3.0$, while holding the other measured values fixed, a closer fit to the experimental data results, but r_{RD} and r_{TD} now have no physical significance (as mentioned earlier). This change results in the revised model parameters:

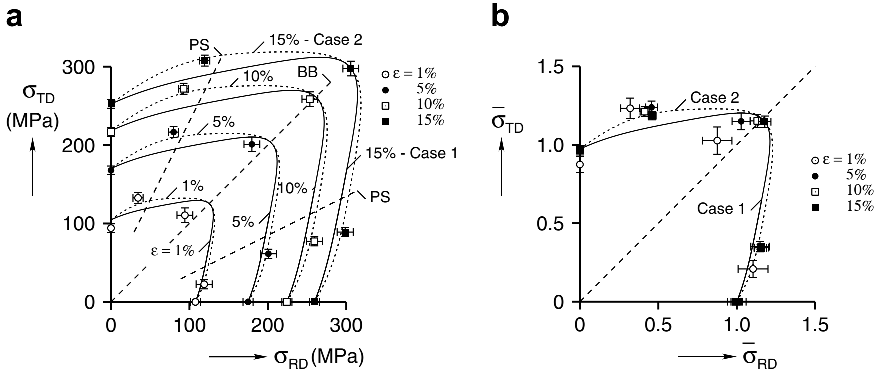

Fig. 13. Equal plastic work yield stress data from Fig. 11a, and normalized values from Fig. 12b, both with Yld2000-2d predictions for Case 1, measured *r* values (solid curves) and Case 2, artificially large *r* values (dotted curves).

$$\alpha_1 = 0.8837, \quad \alpha_2 = 1.1993, \quad \alpha_3 = 0.8542, \quad \alpha_4 = 0.8897,$$
$$\alpha_5 = 0.9227, \quad \alpha_6 = 0.6599, \quad \alpha_7 = 0.9775, \quad \text{and} \quad \alpha_8 = 1.4077$$

and the second yield locus curve plotted in Fig. 13b (Case 2, dotted line). Fig. 13a shows these same cases plotted at the all work levels on true stress axes (similar to Fig. 11). These predictions do not fit the PS values for the measured *r* values (Case 1), but are much closer for the artificial *r* values. However, neither Case 1 nor Case 2 capture the behavior for <15% strain. It would seem that the model parameters would have to change with strain hardening to match all the work levels shown.

5. Conclusion

Experimental results for multiple tensile strain states (uniaxial, plane strain, and balanced biaxial) using X-ray diffraction as the measure of stress are shown. The uniaxial data compares well with typical uniaxial tests, verifying the measured effective X-ray elastic constants used. Repeat tests show consistent results in measured values and trends for all the tests performed. The yield surfaces show similar trends to those predicted by a basic von Mises' model, but some behaviors are unique, especially in the balanced biaxial direction. Comparison to the Hill'48 and Hosford'79 models showed little improvement over the von Mises' model. The Yld2000-2d model (with eight parameters) is able to model the balanced biaxial results for a given level of work, but under predicts the plane strain data for the measured plastic strain ratio, *r*, values. Future work is planned to include a detailed investigation of the effect of texture changes on the mechanical behavior using polycrystalline modeling.

Acknowledgements

The authors would like to thank T. Hamblin and T. Warren (Alcan International Ltd.) for supplying the material used in this study, and F. Barlat (Pohang University of Science and Technology) for calculation of the Yld2000-2d model parameters.

References

Banabic, D., 2004. Anisotropy and formability of AA5182-O aluminum alloy sheets. Annals of the CIRP 53 (1), 219–222.

Banovic, S.W., Foecke, T., 2003. Evolution of strain-induced microstructure and texture in commercial aluminum sheet under balanced biaxial stretching. Metallurgical and Materials Transactions A 34 (3), 657–671.

Banovic, S.W., Iadicola, M.A., Foecke, T., 2008. Textural development of AA 5754 sheet deformed under in-plane biaxial tension. Metallurgical and Materials Transactions A, accepted for publication.

Barlat, F., Brem, J.C., Yoon, J.W., Chung, K., Dick, R.E., Lege, D.J., Pourgoghrat, F., Choi, S.H., Chu, E., 2003. Plane stress yield function for aluminum alloy sheets – Part 1: theory. International Journal of Plasticity 19, 1297–1319.

Dölle, H., Hauk, V., Kockelmann, H., Sesemann, H., 1977. X-ray stress measurement on steels having preferred-orientation. Journal of Strain Analysis 12 (1), 62–65.

Flores, P., Duchêne, L., Bouffioux, C., Lelotte, T., Henrard, C., Pernin, N., Van Bael, A., He, S., Duflou, J., Habraken, A.M., 2007. Model identification and FE simulations: effect of different yield loci and hardening laws in sheet forming. International Journal of Plasticity 23, 420–449.

Foecke, T., Banovic, S.W., Fields, R.J., 2001. Sheet metal formability studies at the National Institute of Standards and Technology. JOM 53 (2), 27–30.

Foecke, T., Iadicola, M.A., Lin, A., Banovic, S.W., 2007. A method for direct measurement of multiaxial stress–strain curves in sheet metal. Metallurgical and Materials Transactions A 38A (2).

Gnaeupel-Herold, T., Prask, H.J., Fields, R.J., Foecke, T.J., Xia, Z.C., Lienert, U., 2004. A synchrotron study of residual stresses in a Al6022 deep drawn cup. Materials Science and Engineering A 366, 104–113.

Gutscher, G., Wu, H.-C., Ngaile, G., Altan, T., 2004. Determination of flow stress for sheet metal forming using the viscous pressure bulge (VPB) test. Journal of Materials Processing Technology 146 (1), 1–7.

Hosford, W.F., Caddell, R.M., 1983. Metal Forming: Mechanics and Metallurgy. Prentice-Hall.

Iadicola, M.A., Gnaeupel-Herold, T.H., 2008. In situ stress measurement of biaxially strained AA 5754-O. Advances in X-ray Analysis 51, in press.

Kang, J., Wilkinson, D.S., Jain, M., Embury, J.D., Beaudoin, A.J., Kim, S., Mishira, R., Sachdev, A.V., 2006. On the sequence of inhomogeneous deformation processes occurring during tensile deformation of strip cast AA5754. Acta Materialia 54, 209–218.

Kuwabara, T., 2007. Advances in experiments on metal sheets and tubes in support of constitutive modeling and forming simulations. International Journal of Plasticity 23, 385–419.

Kuwabara, T., Van Bael, A., Iizuka, E., 2002. Measurement and analysis of yield locus and work hardening characteristics of steel sheets with different *r*-values. Acta Materialia 50 (14), 3717–3729.

Kuwabara, T., Yoshida, K., Narihara, K., Takahashi, S., 2005. Anisotropic plastic deformation of extruded aluminum alloy tube under axial forces and internal pressure. International Journal of Plasticity 21, 101–117.

Marciniak, Z., Kuczyński, K., 1967. Limit strains in the processes of stretch-forming sheet metal. International Journal of Mechanical Science 9, 609–620.

Marion, R.H., Cohen, J.B., 1974. Anomalies in measurement of residual stress by X-ray diffraction. Advances in X-ray Analysis 18, 466–501.

Noyan, I.C., Cohen, J.B., 1987. Residual Stress: Measurement by Diffraction and Interpretation. Springer-Verlag.

Ofenheimer, A., Kitting, D., Iadicola, M.A., Foecke, T., 2007. A critical review of different experimental approaches to calibrate numerical sheet forming simulations. In: Proceedings of the Society of Automotive Engineers SP-2103, Society of Automotive Engineers Inc., pp. 331–340.

Raghavan, K.S., 1995. A simple technique to generate in-plane forming limit curves and selected applications. Metallurgical and Materials Transactions A 26A (8), 2075–2084.

Vegter, H., van den Boogaard, A.H., 2006. A plane stress yield function for anisotropic sheet metal by interpolation of biaxial stress states. International Journal of Plasticity 22, 557–580.